A FRAMEWORK FOR VERIFICATION OF SIGNAL PROPAGATION THROUGH SEQUENTIAL NANOMAGNET LOGIC DEVICES

by
Alexander Gunter

A thesis submitted to the faculty of The University of Mississippi in partial fulfillment of the requirements of the Sally McDonnell Barksdale Honors College.

Oxford
December 2016

Approved by

Advisor: Professor Matthew Morrison

Reader: Professor Conrad Cunningham

Reader: Professor Adam Smith

ACKNOWLEDGEMENTS

I first would like to thank the Honors College, Department of Electrical Engineering, and the Department of Computer and Information science for working together to fund my trip to present my work at the Design Automation Conference. The exposure to the field of design automation was invaluable to my project and my future studies.

Thank you to Dr. Matthew Morrison for supporting and guiding me for two years. His patience and advice taught me how to focus on the end goal and get the job done. I could not have even started this project without him.

Finally, thank you to my parents for nurturing my love for science throughout my life. Without their love and reassurance, I would not be here today.

ABSTRACT

Nanomagnet Logic is an emerging technology for low-power, highly-scalable implementation of quantum-dot cellular automata. Feedback permits reuse of logical subroutines, which is a desired functionality of any computational device. Determining whether feedback is feasible is essential to assessing the robustness of nanomagnet logic in any pipelined computing design. Therefore, development of a quantitative approach for verification of feedback paths is critical for development of design and synthesis tools for nanomagnet logic structures. In this paper, a framework for verification of sequential nanomagnet logic devices is presented. A set of definitions for canonical alignment and state definitions for NML paths are presented, as well as mathematical operations for determining the resulting states. The simulation results are presented for quantification of the NML magnetization angles for horizontal, vertical, negative-diagonal, and positive diagonal geometric alignments. The presented framework may be used as the basis for defining a representation of signal propagation for design and verification for robust NML devices and preventing deadlock resulting from improper implementation.

TABLE OF CONTENTS

ACKNOWLEDGEMENTS iii

ABSTRACT iv

LIST OF TABLES vi

LIST OF FIGURES vii

CHAPTER 1: INTRODUCTION 1

CHAPTER 2: NML DEVICES AND PREVIOUS WORK 4

CHAPTER 3: SIMULATION PROCEDURE 10

CHAPTER 4: SIMULATION AND CALCULATION RESULTS 13

CHAPTER 5: APPLICATION OF RESULTS 17

CHAPTER 6: CONCLUSION 20

BIBLIOGRAPHY 21

LIST OF TABLES

Table 1 Magnetization Angles for Single NML Magnets

Table 2 Magnetization Angles for Horizontal Alignment

Table 3 Magnetization Angles for Vertical Alignment

Table 4 Magnetization Angles for Negative-Diagonal Alignment

Table 5 Magnetization Angles for Positive-Diagonal Alignment

LIST OF FIGURES

Figure 1	Example of a Phase Diagram
Figure 2	Illustration of NML Clocking Zones
Figure 3	Grid Placements of NML Magnets
Figure 4	Simulation of Single NML Magnets and Illustration of Shape-Based Logic Gates
Figure 5	Simulation of NML Magnet Pairs

CHAPTER 1

INTRODUCTION

Nanomagnet logic (NML) is an emerging technology implementing quantum-dot cellular automata (QCA) for highly scalable, radiation-hard logic structures that retain states without consuming power and dissipate little energy during state changes [1]. NML encodes binary data in magnetic polarizations and performs operations via fringing field interactions. As the data signal propagates through an NML devices, magnetic polarizations permit non-volatile implementation in systolic architectures [2], [3]. Combinational NML devices, such as 2-input AND [4] and OR gates [5], inverters, and devices with fanout [6], enabling on-chip clocking for mature devices at room temperature [7].

The key characteristic of NML is use of elongated nanomagnets, each of which features a bistable field [8]. NML is intrinsically pipelined, which permits high-throughput systolic architecture, but requires a number of clock phases over a NML interconnect. For a lone nanomagnet, the stable states are polarized along the longer axis of the magnet, angled either 90° or -90° to the shorter axis. Increasing the horizontal component of the magnetic field surrounding a magnet will shift this angle towards horizontal, and a phase diagram can illustrate the precise relationship between the external field and the angle of magnetization. Given a phase diagram as described in [27], the states ‘Up,’ ‘Down,’ and ‘Metastable’ may be assigned to appropriate ranges of angles with Metastable centered near 0°.

Estimates for on-chip power consumption of billions of NML switches at 100MHz show the possibility for devices consuming less than 0.1W [9]. However, because the energy difference between the Up and Down states can be very large, NML needs an external clocking field to reevaluate nanomagnet states for new inputs [10]. External clocking fields are partitioned into separate regions called clocking zones, which control small neighborhoods of nanomagnets in order to prevent errors and better control data propagation [11]. The clocking zones are activated in series, iteratively pushing their respective nanomagnets to the metastable state before letting them fall back to the correct binary states.

Regulating NML bistable fields using external clocking fields will permit efficient implementation of sequential QCA devices, particularly in implementations where power dissipation may be exploited, such as Differential Power Analysis [12]. Analysis of power dissipation in QCA is significant [13-15]. However, quantification of the implications of external clocking fields in pipelined elements has only been recently investigated in a few cases [16-22] due to NML technology not being mature. A framework for verification of magnetic signal propagation through sequential NML must be developed in order to mitigate significant performance and signal synchronization challenges.

In this paper, a framework for quantifying signal propagation along NML wires comprised of square nanomagnets in sequential designs is presented, with a primary purpose of verification of NML sequential circuits. The framework verifies logical correctness and support of sequential elements given a set of clocking zones. The model mirrors the behavior of general NML circuits with high fidelity, functioning, and circuit

failure. In this paper, simulation data from multiple NML arrangements and inputs are presented as the foundation for a data representation of NML, which will bypass the computational complexity of physical simulation by describing ideal behavior indicated by simulation data. In Section II, the fundamental physical principles of NML circuits, their interactions given placement and shape are reviewed. In Section III, we present our procedure for simulating data propagation between square magnets and a summary of our results. In Section IV, simulation data is used to define the foundation for a computational model of sequential NML and is capable of representing the adjacencies and logical states of square and rectangular nanomagnets. The model will additionally be capable of calculating the evolution of elementary NML circuits. In Section V, avenues for future work are discussed, including refinement of this data representation to support general NML circuits and Sequential Reversible Nanomagnet Logic (SRNML).

CHAPTER 2

NML DEVICES AND PREVIOUS WORK

Sequential computation is the use of outputs in successive calculations [22] and is realized by making one or more inputs dependent on one or more outputs. Sequential logic structures are physically implemented with feedback wires from the outputs to the inputs, and must preserve data between clocking cycles. Resultantly, each output signal is dependent on the previous outputs, and not only depends on the current set of inputs but also the exact sequence of inputs leading up to the current one. Support of feedback wires in NML is dependent on both placement of nanomagnets and the order in which they are clocked. Any model of NML must support identification of combinations of nanomagnet placements and clocking mechanisms where feedback is not permissible.

Basic nanomagnet logic operates on the fringing field interactions between bistable nanomagnets [23]. For such a nanomagnet placed in an externally produced magnetic field, there will be states for that nanomagnet, in the form of angles of polarization, which minimize total energy. However, if that field is not strong enough, the nanomagnet will not necessarily reside in that state. A phase diagram, as shown in Figure 1, illustrates the relationship between the external field and most stable angle of polarization. Using this diagram, we can assign the labels 'Up,' 'Down,' and 'Metastable' to appropriate ranges of angles with Metastable being a neutral state only possible in a strong horizontal field.

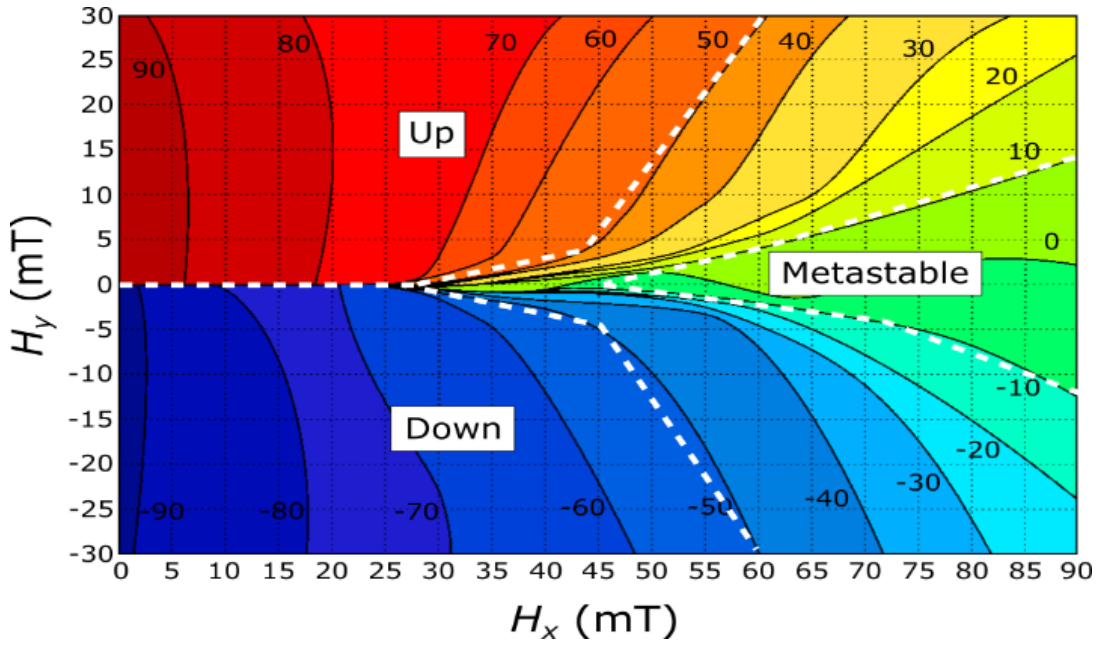

Figure 1: An example of a phase diagram for some rectangular nanomagnet. H_x and H_y are the horizontal and vertical components of the external magnet field. Given a phase diagram, ranges of magnetization angles map to the states Up, Down, and Metastable.

By placing nanomagnets appropriately, NML structures may be built which define such stable states and behave according to Boolean algebra and digital circuitry. Nanomagnets are restricted to a grid, and wires are horizontal or vertical chains. Rectangular nanomagnets placed horizontally align antiferromagnetically, and thus each nanomagnet in a horizontal wire acts as a Boolean NOT operator. Due to the additive nature of magnetic fields, nanomagnets behave according to a majority voter function. Given a set of neighboring magnets, a nanomagnet's most stable state will align with the state held by the majority its neighbors. In the event of a tie, both Up and Down will be equally stable; so a rectangular nanomagnet will randomly choose between the two. The AND and OR operators can be built from majority gates. Alternatively, AND and OR operators can be built by using trapezoidal magnets which are effectively biased towards one state [29]. All of these operators and implementations have been experimentally

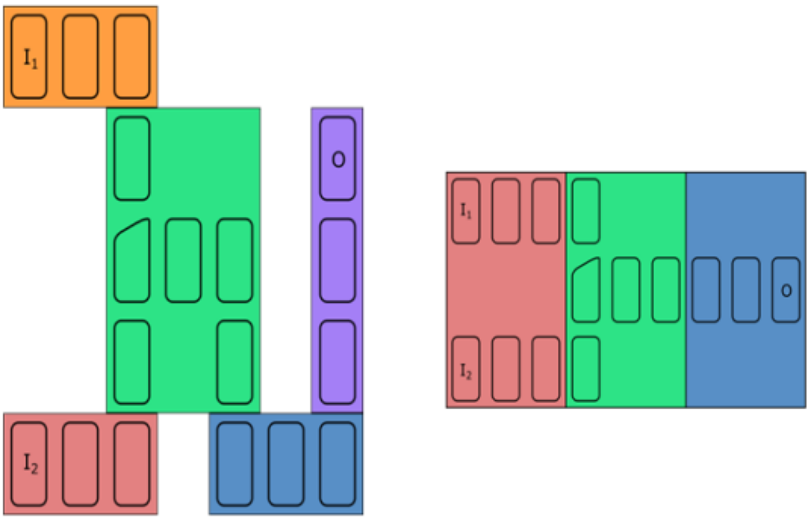

Figure 2: (a) NML circuit with 2 inputs and 1 output, divided into clocking zones according to a standard cell library as described in [30]. (b) NML circuit implemented with a snake clock where clocking zones are bounded in only one direction. In this example, clocking zones are bounded horizontally and extend vertically along the entire length of the circuit.

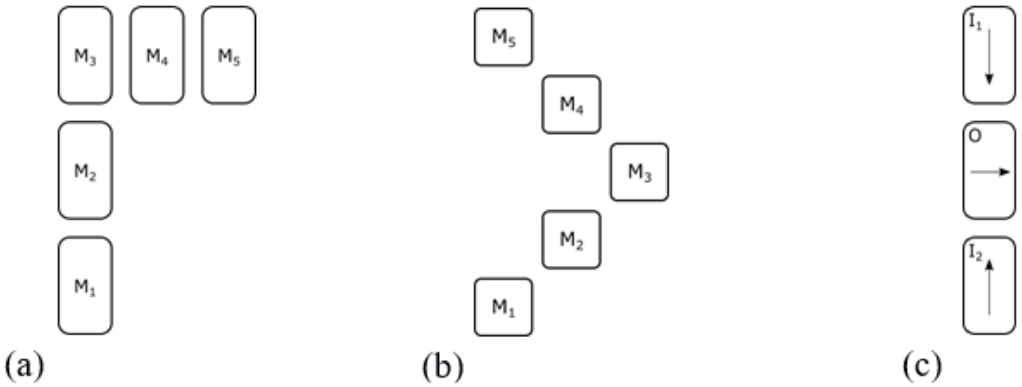

Figure 3: (a)-(b) Nanomagnets placed on valid grid locations, both horizontally and diagonally (c) When two inputs feed opposing states into a Metastable rectangular output, the output experiences a tie vote and will randomly choose between the two.

demonstrated, so the presented model must support the definition of classes of magnets which behave according to an input set of rules.

NML structures and designs are not limited to elongated rectangular shapes. Alternate implementations of the AND and OR operators, as well as a crossover gate which lets two wires cross each other [24, 25]. The AND and OR alternatives use a

trapezoidal shape which biases the nanomagnet towards one direction. The crossover is implemented with an ensemble of five square nanomagnets arranged in a cross pattern. Each design permits horizontal, vertical, or diagonal polarization; and the entire structure is rotated 45°. The resulting alignment between the square magnets and any coupled rectangular magnets becomes 45° as well, instead of 90° and 0°. The square magnets will still behave according to a majority function, polarizing in the direction that minimizes total energy, but a model of NML must be able to represent polarization and alignment in all eight directions. Table 1 shows the magnetization angles for single magnets, where θ_H and φ_H are respectively the azimuthal and polar angles of the external magnetic field, θ_M and φ_M are respectively the azimuthal and polar angles of the nanomagnet's average magnetization, and ε_θ represents the amount by which θ_M deviates from the azimuthal angle of the nearest canonical state. All five of these measurements are in degrees. Examples of coupled square and rectangular alignment, as well as trapezoidal implementations of AND and OR gates, are shown in Figure 4.

Nanomagnets do not easily switch between the Up and Down states due to significant energy difference between the two. The logically correct state rests around 4×10^{-19} *J*, and the incorrect state is near 7×10^{-19} *J* [27]. The Metastable state separates them at 9×10^{-19} *J*. In order to reevaluate an NML circuit for new inputs, an external clocking field must force the nanomagnets into the Metastable state before letting them fall into the correct state. To minimize errors, this clocking mechanism must be applied to small sets of nanomagnets in sequence rather than all at once [26]. Clocking zones are single, continuous areas that contain the set of nanomagnets in a logic structure whose clocking fields are activated simultaneously. The standard three-step process for

$\boldsymbol{\theta_F}$	$\boldsymbol{\varphi_F}$	$\boldsymbol{\theta_M}$	$\boldsymbol{\varphi_M}$	$\boldsymbol{\varepsilon_\theta}$
0.00	0.00	0.00	0.00	0.00
0.00	90.00	0.00	90.00	0.00
45.00	90.00	45.00	90.00	0.00
90.00	90.00	90.00	90.00	0.00
135.00	90.00	135.00	90.00	0.00
180.00	90.00	180.00	90.00	0.00
225.00	90.00	225.00	90.00	0.00
270.00	90.00	270.00	90.00	0.00
315.00	90.00	315.00	90.00	0.00

Table 1: Magnetization angles for single NML magnets. All columns are in degrees.

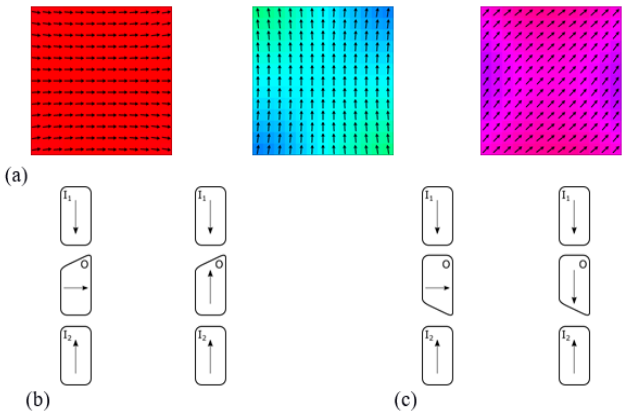

Figure 4: OOMMF simulations of single square nanomagnets exhibiting magnetization states of $\theta_M = 0°$, $\theta_M = 90°$, and $\theta_M = 45°$ with $\varphi_M = 90°$. (b) A shape-based majority gate defaulting to the UP state described by $\theta_M = 90°$, $\varphi_M = 90°$. If UP maps to Boolean True, this is an OR Gate. (c) A shape-based majority gate defaulting to the DOWN state described by $\theta_M = 0°$, $\varphi_M = 90°$. If DOWN maps to Boolean False, this is an AND Gate.

activating clocking zones is to first turn on the clock for one zone, then the clock for an adjacent zone, and finally turning off the clock for the initial zone. The clocking zone activation process has the effect of pulling the data from the first zone's neighbors and into that zone without the next zone's nanomagnets affecting the new state. Iteratively

applying this process to a wire sends data in the direction that clocking is applied. Thus, the order that zones are clocked in affects the direction that data flows and the order that logic is applied. This in turn directly affects a NML circuit's behavior. Our model must account for this clocking order and how it affects other characteristics of the circuit.

CHAPTER 3

SIMULATION PROCEDURE

Since sequential logic structures must successfully hold a logic signal while simultaneously minimizing delay, development of a verification framework for sequential NML requires consideration of magnet shape, propagation of clocking zones, and placement geometry. In this section, the proposed simulation procedure is detailed. A set of definitions for clarification and our simulation parameters are specified in order to meet these requirements. The section ends with the calculation used to extract the data we need to build our data representation of NML.

3.1 Preliminary Definitions

First we present a set of definitions for describing data propagation along NML wires for clarification.

Input Magnet: A magnet that receives an input signal from some source external to the NML circuit.

Input State: The state possessed by a given input magnet after it has received its input.

Output Magnet: A magnet from which no other magnets receive input.

Output State: The state possessed by a given output magnet after it has received its input.

Magnet Alignment: Given two adjacent magnets, the parametric line passing through the points at which each magnet is closest to the other.

Canonical Alignment: A magnet alignment f(t) of the Cartesian form $\langle t, 0, 0\rangle$, $\langle 0, t, 0\rangle$, $\langle 0, 0, t\rangle$, $\langle t, t, 0\rangle$, or $\langle t, -t, 0\rangle$.

Canonical State: A magnetization state which lies on one of the canonical alignments.

All simulations consist of square magnets whose states can rotate about the z-axis. The primary simulations are of two-magnet circuits with one input magnet and one output magnet. The simulations of single magnets are used as a source of constants to be used in later calculations. Magnets are restricted to residing on a square grid on the xy-plane. Given an input magnet, an output magnet may reside in one of the eight surrounding grid cells; and there is a line passing through the nearest corners of each magnet.

The geometric restriction corresponds to four unique magnet alignments on the xy-plane: $\langle t, 0, 0\rangle$, $\langle 0, t, 0\rangle$, $\langle t, t, 0\rangle$, and $\langle t, -t, 0\rangle$. These alignments are defined as Horizontal, Vertical, Positive-Diagonal, and Negative-Diagonal respectively; and we have defined these as canonical alignments. Each canonical alignment has two corresponding canonical states, each pair being additive inverses that extend along a canonical alignment in opposite directions.

3.2 Simulation Setup

Our goal with these simulations is to identify how, given an input state, the alignment between two magnets changes the output state induced by the input magnet in an ideal environment. Thus, all simulations use a minimization evolver rather than a time evolver.

In all cases, the average magnetization of the total system in *A/m* are logged, and they include the contribution from empty space and are not normalized.

All simulations are based on those performed in [27]. The presented simulations use nanomagnets composed of Cobalt with a saturation magnetization of 10^6 *A/m* and an exchange stiffness constant of 1.3×10^{-11} *J/m*. A straight-edged square shape with dimensions 39×39×5 nm^3 was used in the presented simulations. The simulation mesh geometry is 3×3×5 nm^3. The horizontal and vertical distances between nanomagnets are both 9 *nm*, and diagonally placed nanomagnets are $9\sqrt{2}$ *nm* apart at the nearest corners. The two-magnet systems have mesh cells which behave like a vacuum, and the single-magnet systems have no vacuum cells. The simulations in [27] used rectangular nanomagnets are 39×63×5 nm^3.

All magnet states are initialized in this framework to the canonical state $\langle 0, 0, t \rangle$ for positive *t*. The input state is set by a uniform magnetic field of 100 *mT* in the direction of the desired canonical state. This is strong enough to both set the input state and hold that state constant during the simulation. This field is bounded by the edges of the input magnet in the xy-plane. In the two-magnet simulations, the field does not directly influence the output magnet. Tests for nine canonical input states for single magnets were conducted, and all nine were tested against the four proposed canonical alignments of interest for a total of forty-five unique cases. Each case was then run 100 times in simulation.

CHAPTER 4

SIMULATION AND CALCULATION RESULTS

4.1 Calculation Procedure

The simulations presented below were completed using OOMMF, and a program was written in Python to perform all post-simulation calculations. We begin with the single-magnet simulations. The final magnetization of a single-magnet system corresponds to the most stable state of a square nanomagnet with the given input. For a given input state, we average this output from all 100 simulations to produce the average magnetization of a single magnet in that state. For a given input state, this average magnetization is represented by $\widehat{M}_I$.

In the same manner, for each two-magnet test case, we take the average magnetization outputs for all 100 simulations, denoted $\widehat{M}_S$. Then we derive the output magnet's average magnetization by removing the input magnet's and vacuum's contribution to the total average, as in (1):

$$\widehat{M}_O = \frac{(2\alpha+\beta)\widehat{M}_S - \alpha\widehat{M}_I}{\alpha} \qquad (1)$$

where α is the number of mesh cells contained within a square nanomagnet, and β is the number of cells contained within the vacuum in the simulation. $\alpha = 169$ for our chosen nanomagnet and mesh cell dimensions. $\beta = 39$ in the horizontal and vertical tests, and $\beta = 503$ in the diagonal tests.

After calculating the average magnetization of the output magnets, the output states are converted and canonical states to spherical coordinates. Then, the difference in azimuthal angle θ and polar angle φ between each output state and its nearest canonical state are determined.

4.2 Magnetization Standard Deviations and Averages

The presented single-magnet simulations were highly consistent with standard deviations generally ranging from 1.22×10^{-13} *A/m* to 1.18×10^{-6} *A/m*. All data for the z-component of magnetization and the data for the test case $\theta = 0, \varphi = 0$ had no deviation. Near-zero average magnetizations had components on the order of 10^{-12} *A/m*. Averages for $|\widehat{M}_I|$ were on the order of 10^{6} *A/m*. Average magnetization angles in degrees for single-magnet simulations are shown in Table 1.

The presented two-magnet simulations displayed more inconsistency overall. Non-zero standard deviations ranged from 1.49×10^{-12} *A/m* to 1.53×10^{-3} *A/m*. Of particular note is that diagonal alignments featured standard deviations in the middle of this range, from 8.21×10^{-10} *A/m* to 8.56×10^{-5} *A/m*. The Horizontal and Vertical alignments featured standard deviations ranging from both extremes. Averages for $|\widehat{M}_O|$ were on the order of 10^{6} *A/m*. Average magnetization angles for two-magnet simulations are shown in Tables 2 through 5.

θ_I	φ_I	θ_O	φ_O	ε_θ
0.00	0.00	0.00	0.00	0.00
0.00	90.00	0.00	90.00	0.00
45.00	90.00	327.65	90.00	12.65
90.00	90.00	270.00	90.00	0.00
135.00	90.00	212.35	90.00	-12.65
180.00	90.00	180.00	90.00	0.00
225.00	90.00	147.65	90.00	12.65
270.00	90.00	90.00	90.00	0.00
315.00	90.00	32.35	90.00	-12.65

Table 2: Magnetization angles for horizontal alignments. All columns are in degrees.

θ_I	φ_I	θ_O	φ_O	ε_θ
0.00	0.00	0.00	0.00	0.00
0.00	90.00	180.00	90.00	0.00
45.00	90.00	122.35	90.00	-12.65
90.00	90.00	90.00	90.00	0.00
135.00	90.00	57.65	90.00	12.65
180.00	90.00	0.00	90.00	0.00
225.00	90.00	302.35	90.00	-12.65
270.00	90.00	270.00	90.00	0.00
315.00	90.00	237.65	90.00	12.65

Table 3: Magnetization angles for vertical alignment. All columns are in degrees.

θ_I	φ_I	θ_O	φ_O	ε_θ
0.00	0.00	0.00	0.00	0.00
0.00	90.00	308.06	90.00	-6.94
45.00	90.00	225.00	90.00	0.00
90.00	90.00	141.94	90.00	6.94
135.00	90.00	135.00	90.00	0.00
180.00	90.00	128.06	90.00	-6.94
225.00	90.00	45.00	90.00	0.00
270.00	90.00	321.94	90.00	6.94
315.00	90.00	315.00	90.00	0.00

Table 4: Magnetization angles for negative-diagonal alignment. All columns are in degrees.

θ_I	φ_I	θ_O	φ_O	ε_θ
0.00	0.00	0.00	0.00	0.00
0.00	90.00	51.94	90.00	6.94
45.00	90.00	45.00	90.00	0.00
90.00	90.00	38.06	90.00	-6.94
135.00	90.00	315.00	90.00	0.00
180.00	90.00	231.94	90.00	6.94
225.00	90.00	225.00	90.00	0.00
270.00	90.00	218.06	90.00	-6.94
315.00	90.00	135.00	90.00	0.00

Table 5: Magnetization angles for positive-diagonal alignment. All columns are in degrees.

CHAPTER 5

APPLICATION OF RESULTS

The results generated from the presented simulation framework indicate that certain canonical alignments are more inefficient at transmitting certain canonical states. In all tests, output for a given canonical magnet alignment displayed negligible deviation from canonical states for input states parallel or perpendicular to the magnet alignment. Input states which were angled 45° away from parallel or perpendicular produced outputs with large deviations. Specifically, the Positive-Diagonal and Negative-Diagonal magnet alignments produced outputs which deviated by 6.94° from the nearest canonical states when the input state was Horizontal or Vertical. The outputs for Vertical and Horizontal magnet alignments deviated by 12.65° when the input states where Positive-Diagonal or Negative-Diagonal. Figure 5 illustrates these deviations.

Although these tests demonstrate deviation from canonical states, those deviations are highly consistent and are bisected by canonical states. Based on [31], this deviation may be reduced with modifications to magnet shape in order to increase the stability of canonical states. In such a case, we can use these measurements as a foundation for a computational framework of NML. If the model is only concerned with NML wires and foregoes modeling of logic gates, the magnet state may be represented as the Kronecker product of two column vectors of three elements each where every element is a Boolean value, and exactly one element in each vector is true. Each vector represents the magnet's alignment along the x and y axis respectively, and the single true value in the cross

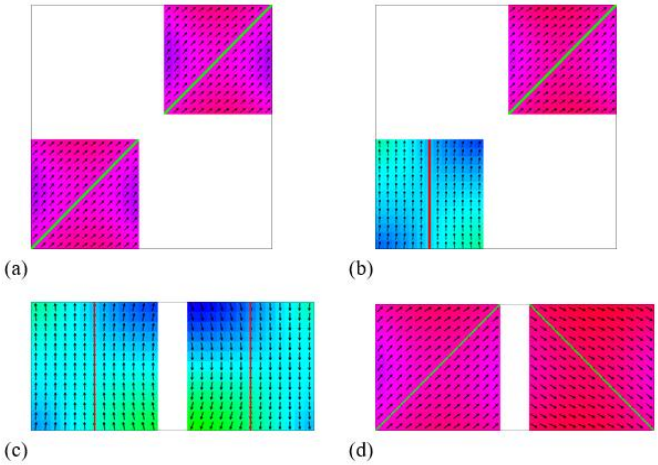

Figure 5: (a) OOMMF simulations of a diagonal state transmitted diagonally result in minimal deviation from the canonical states parallel to the green overlaid lines. The input magnet is on the left, and the output magnet is on the right. (b) A vertical input transmitted diagonally results in a small increase in deviation by 6.94°. (c) Horizontal transmission of vertical states produces an average magnetization with minimal deviation. (d) Horizontal transmission of diagonal states results in a larger deviation by 12.65°.

product corresponds to a canonical state. (2) presents one possible representation.

$$S = [x_U, x_\emptyset, x_D]^T \otimes [y_U, y_\emptyset, y_D]^T \qquad (2)$$

The data transmissions are representable as matrix multiplication where the alignment matrix *M* corresponds to the magnet alignment and transforms the state vector *S* based upon our simulation results. Using the state representation presented by (2) thus yields the horizontal and vertical alignment matrices (3) and (4).

$$H = \begin{bmatrix} 1 & 0 & 0 \\ 0 & 1 & 0 \\ 0 & 0 & 1 \end{bmatrix} \otimes \begin{bmatrix} 0 & 0 & 1 \\ 0 & 1 & 0 \\ 1 & 0 & 0 \end{bmatrix} \qquad (3)$$

$$V = \begin{bmatrix} 0 & 0 & 1 \\ 0 & 1 & 0 \\ 1 & 0 & 0 \end{bmatrix} \otimes \begin{bmatrix} 1 & 0 & 0 \\ 0 & 1 & 0 \\ 0 & 0 & 1 \end{bmatrix} \qquad (4)$$

These matrices correspond to each alignment's tendency to invert one Cartesian component of a magnet state while not affecting the other component. For example, it is known that horizontal wires invert vertical states [28]; and our simulations demonstrated this behavior. Simulation data indicates that this inversion holds for diagonal states as well, although less stably for straight-edge square magnets. Thus alignment matrices D_P and D_N may also be defined for the diagonal alignments, although they are not so easily factored. Just like (3) and (4), (5) and (6) are based on the representation presented in (2).

$$D_P = \begin{bmatrix} 1 & 1 & 0 & 1 & 0 & 0 & 0 & 0 & 0 \\ 0 & 0 & 0 & 0 & 0 & 0 & 0 & 0 & 0 \\ 0 & 0 & 0 & 0 & 0 & 0 & 1 & 0 & 0 \\ 0 & 0 & 0 & 0 & 0 & 0 & 0 & 0 & 0 \\ 0 & 0 & 0 & 0 & 1 & 0 & 0 & 0 & 0 \\ 0 & 0 & 0 & 0 & 0 & 0 & 0 & 0 & 0 \\ 0 & 0 & 1 & 0 & 0 & 0 & 0 & 0 & 0 \\ 0 & 0 & 0 & 0 & 0 & 0 & 0 & 0 & 0 \\ 0 & 0 & 0 & 0 & 0 & 1 & 0 & 1 & 1 \end{bmatrix} \quad (5)$$

$$D_N = \begin{bmatrix} 0 & 0 & 0 & 0 & 0 & 0 & 0 & 0 & 1 \\ 0 & 0 & 0 & 0 & 0 & 0 & 0 & 0 & 0 \\ 0 & 1 & 1 & 0 & 0 & 1 & 0 & 0 & 0 \\ 0 & 0 & 0 & 0 & 0 & 0 & 0 & 0 & 0 \\ 0 & 0 & 0 & 0 & 1 & 0 & 0 & 0 & 0 \\ 0 & 0 & 0 & 0 & 0 & 0 & 0 & 0 & 0 \\ 0 & 0 & 0 & 1 & 0 & 0 & 1 & 1 & 0 \\ 0 & 0 & 0 & 0 & 0 & 0 & 0 & 0 & 0 \\ 1 & 0 & 0 & 0 & 0 & 0 & 0 & 0 & 0 \end{bmatrix} \quad (6)$$

With this representation, the output of an n-magnet wire can be calculated as

$$\hat{S}_O = M_{n-1} M_{n-2} \ldots M_1 \hat{S}_I \quad (7)$$

where $\hat{S}_I$ is the input state, $\hat{S}_O$ is the output state, and M_i is the matrix corresponding to the *i*-th magnet alignment in the wire. Thus we can approximate data propagation along a NML wire using multiplication of 9x9 matrices and a 9-element column vector.

CHAPTER 6

CONCLUSION

Simulation of sequential NML devices in OOMMF show that square nanomagnets placed on a grid exhibit highly predictable behavior when restricted to specific canonical states. This behavior makes NML wires easily modeled by linear systems. Signal propagation across a wire was approximated with an initial column vector which is transformed by matrices representing the alignment between each pair of magnets in the wire. Verification of appropriate NML layouts and states is made possible through use of this information, and may be implemented in a computational framework for more efficient design and simulation of NML circuits. Development of such a framework will require a state representation which supports logic gates and a representation of NML clocking zones. Investigation of rotations or alternative nanomagnet shapes, such as squares with concave edges, may yield nanomagnets which display less deviation from canonical states than the nanomagnets simulated. We find that the presented representation works well for standalone wires, but using it as a foundation for modeling general NML circuits necessitates many ad hoc rules and definitions.

BIBLIOGRAPHY

[1] Crocker, M.; Hu, X.S.; Niemier, M., "Design and comparison of NML systolic architectures," in *NANOARCH*, pp.29-34, 17-18 June 2010.

[2] Z. Yan and D. V. Sarwate, "New systolic architectures for inversion and division in GF(2m)," IEEE Trans. on Computers, pp. 1514–1519, 2003.

[3] N. Gupta and N. Gupta, "A VLSI architecture for image registration in real time," IEEE Trans. on VLSI Systems, vol. 15, pp. 981–989, 2007.

[4] P. D. Tougaw, C. S. Lent, and W. Porod, "Bistable saturation in coupled quantum-dot cells," J. Appl. Phys., vol. 74, no. 5, pp. 3558–3566, 1993.

[5] A. Imre et al., "Majority logic gate for Magnetic Quantum-dot Cellular Automata," Science, vol. 311 no. 5758, pp. 205–208, January 13, 2006.

[6] M. Niemier et al., "Boolean logic through shape-engineered magnetic dots with slanted edges," *IEEE Trans. on Nanotechnology*, 2010.

[7] E. Varga et al., "Experimental demonstration of fanout for nanomagnet logic," *IEEE Trans. on Nanotechnology*, 2010.

[8] M. T. Alam et al., "On-chip clocking for nanomagnet logic devices," *IEEE Transactions on Nanotechnology*, 2010.

[9] G. Csaba et al., "Simulation of power gain and dissipation in fieldcoupled nanomagnets," J. of Comp. Electronics, vol. 4, pp. 105–110, 2005.

[10] Peng Li; Csaba, G.; Sankar, V.K.; Sharon Hu, X.; Niemier, M.; Porod, W.; Bernstein, G.H., "Power reduction in nanomagnetic logic clocking through high permeability dielectrics," in *2012 DRC*, pp.129-130, 18-20 June 2012.

[11] A. Imre, L. Ji, G. Csaba, A. Orlov, G. H. Bernstein, and W. Porod, "Magnetic logic devices based on field-coupled nanomagnets," in Proc. Int. Semiconductor Device Res. Symp., Dec. 2005, p. 25.

[12] C. Clavier, J.-S. Coron, and N. Dabbous, "Differential power analysis in the presence of hardware countermeasures," in CHES '00. London, UK, UK: Springer-Verlag, 2000, pp. 252–263.

[13] M. Graziano, M. Vacca, A. Chiolerio, and M. Zamboni, “An NCL-HDL snake-clock-based magnetic QCA architecture,” IEEE Trans. Nanotechnol., vol. 10, no. 5, pp. 1141–1149, Sep. 2011.

[14] Y. Gang, W. Zhao, J.-O. Klein, C. Chappert, and P. Mazoyer, “A highreliability, low-power magnetic full adder,” IEEE Trans. Magn., vol. 47, no. 11, pp. 4611–4616, Nov. 2011.

[15] M.P. Frank, “Common mistakes in adiabatic logic design and how to avoid them.” Embedded Systems and Applications, 216-222, 2003.

[16] M. T. Niemier and P. M. Kogge, “Exploring and exploiting wire-level pipelining in emerging technologies,” in *Proc. 28th Annu. Int. Symp. Comput. Archit.*, 2001, pp. 166–177.

[17] W. Liu, L. Lu, M. O’Neill, E. E. Swartzlander, and R. Woods, “Design of quantum-dot cellular automata circuits using cut-set retiming,” *IEEE Trans. Nanotechnol.*, vol. 10, no. 5, pp. 1150–1160, Sep. 2011.\

[18] M. Vacca, M. Graziano, and M. Zamboni, “Asynchronous solutions for nanomagnetic logic circuits,” *ACM J. Emerg. Technol. Comput. Syst.*, vol. 7, no. 4, Dec. 2011, Art. ID 15.

[19] P. Venkataramani, S. Srivastava, and S. Bhanja, “Sequential circuit design in quantum-dot cellular automata,” in *Proc. 8th IEEE Conf. Nanotechnol. (NANO)*, Aug. 2008, pp. 534–537.

[20] Vacca, M.; Juanchi Wang; Graziano, M.; Roch, M.R.; Zamboni, M., "Feedbacks in QCA: A Quantitative Approach," in *Very Large Scale Integration (VLSI) Systems, IEEE Transactions on* , vol.23, no.10, pp.2233-2243, Oct. 2015.

[21] Thapliyal, H. and Ranganathan, N. 2010. "Design of reversible sequential circuits optimizing quantumcosts, delay, and garbage outputs." ACM J. Emerg. Technol. Comput. Syst. 6, 4, Article 14 (December 2010).

[22] M. Morrison and N. Ranganathan, “Analysis of Sequential Reversible Logic Structures using Quantum Mechanics Principles”, ISVLSI, 2012, pp. 219-224.

[23] Perricone, R.; Liu, Y.; Dingler, A.; Hu, X.S.; Niemier, M., "Design of Stochastic Computing Circuits using Nanomagnetic Logic," in *Nanotechnology, IEEE Transactions on* , vol.PP, no.99, pp.1-1.

[24] Siddiq, M.A.; Niemier, M.T.; Csaba, G.; Hu, X.S.; Porod, W.; Bernstein, G.H., "Demonstration of Field-Coupled Input Scheme on Line of Nanomagnets," in *Magnetics, IEEE Transactions on* , vol.49, no.7, pp.4460-4463, July 2013.

[25] Dey, H.; Csaba, G.; Hu, X.S.; Niemier, M.; Bernstein, G.H.; Porod, W., "Switching Behavior of Sharply Pointed Nanomagnets for Logic Applications," in *Magnetics, IEEE Transactions on* , vol.49, no.7, pp.3549-3552, July 2013.

[26] D'Souza N., Salehi-Fashami M., Bandyopadhyay S. & Atulasimha J. Experimental clocking of nanomagnets with strain for ultra low power Boolean logic. arXiv:1404.2980.

[27] Palit, Indranil; Hu, X.Sharon; Nahas, Joseph; Niemier, Michael, "Systematic design of Nanomagnet Logic circuits," in *Design, Automation & Test in Europe Conference & Exhibition (DATE), 2013* , vol., no., pp.1795-1800, 18-22 March 2013.

[28] M. T. Niemier et al., "Nanomagnet logic: progress toward system-level integration," in *J of Physics: Condensed Matter*, vol. 23, no. 49, p. 493202, 2011.

[29] Niemier, M.T.; Alam, M.T.; Bernstein, G.H.; Hu, X.S.; Porod, W.; Varga, E., "Non-Majority MQCA Magnetic Logic Gates and Arrays Based on Misaligned Magnetic Islands," U.S. Patent 8 058 906, November 15, 2011.

[30] Feller, A.; Noto, R.; Smith, A.M., "Standard cell approach for generating custom CMOS/SOS devices using a fully automatic layout program," in *Circuits & Systems Magazine* , vol.3, no.3, pp.9-13, Sept. 1981.

[31] B.J. Lambson, Energy Efficient Digital Logic Using Nanoscale Magnetic Devices. *UC Berkeley: Electrical Engineering & Computer Sciences*. Spring 2013. Retrieved from: http://escholarship.org/uc/item/6263p0wz